

RESEARCH ARTICLE

10.1002/2016JB013925

Special Section:

Slow Slip Phenomena and Plate Boundary Processes

Key Points:

- A robust automatic tremor detection and location algorithm for the southern Central Range of Taiwan
- Observations of a short-term increase in the tremor rate starting at 19 days before a nearby M_L 6.4 earthquake
- No GPS signals associated with tremor activity in the southern Central Range

Supporting Information:

- Supporting Information S1

Correspondence to:

K. Chao,
kchao@northwestern.edu

Citation:

Chao, K., Z. Peng, Y.-J. Hsu, K. Obara, C. Wu, K.-E. Ching, S. van der Lee, H.-C. Pu, P.-L. Leu, and A. Wech (2017), Temporal variation of tectonic tremor activity in southern Taiwan around the 2010 M_L 6.4 Jiashian earthquake, *J. Geophys. Res. Solid Earth*, 122, 5417–5434, doi:10.1002/2016JB013925.

Received 1 JAN 2017

Accepted 23 JUN 2017

Accepted article online 27 JUN 2017

Published online 22 JUL 2017

Temporal variation of tectonic tremor activity in southern Taiwan around the 2010 M_L 6.4 Jiashian earthquakeKevin Chao^{1,2,3} , Zhigang Peng⁴ , Ya-Ju Hsu⁵ , Kazushige Obara⁶ , Chunquan Wu⁷ , Kuo-En Ching⁸, Suzan van der Lee³, Hsin-Chieh Pu⁹, Peih-Lin Leu⁹, and Aaron Wech¹⁰ 

¹Northwestern Institute on Complex Systems, Northwestern University, Evanston, Illinois, USA, ²Center for Optimization and Statistical Learning, Northwestern University, Evanston, Illinois, USA, ³Department of Earth and Planetary Sciences, Northwestern University, Evanston, Illinois, USA, ⁴School of Earth and Atmospheric Sciences, Georgia Institute of Technology, Atlanta, Georgia, USA, ⁵Institute of Earth Sciences, Academia Sinica, Taipei, Taiwan, ⁶Earthquake Research Institute, University of Tokyo, Tokyo, Japan, ⁷Center for Earthquake Research and Information, University of Memphis, Memphis, Tennessee, USA, ⁸Department of Geomatics, National Cheng Kung University, Tainan, Taiwan, ⁹Central Weather Bureau, Taipei, Taiwan, ¹⁰U.S. Geological Survey, Anchorage, Alaska, USA

Abstract Deep tectonic tremor, which is extremely sensitive to small stress variations, could be used to monitor fault zone processes during large earthquake cycles and aseismic processes before large earthquakes. In this study, we develop an algorithm for the automatic detection and location of tectonic tremor beneath the southern Central Range of Taiwan and examine the spatiotemporal relationship between tremor and the 4 March 2010 M_L 6.4 Jiashian earthquake, located about 20 km from active tremor sources. We find that tremor in this region has a relatively short duration, short recurrence time, and no consistent correlation with surface GPS data. We find a short-term increase in the tremor rate 19 days before the Jiashian main shock, and around the time when the tremor rate began to rise one GPS station recorded a flip in its direction of motion. We hypothesize that tremor is driven by a slow-slip event that preceded the occurrence of the shallower Jiashian main shock, even though the inferred slip is too small to be observed by all GPS stations. Our study shows that tectonic tremor may reflect stress variation during the pre-nucleation process of a nearby earthquake.

1. Introduction

Deep tectonic tremor is a newly discovered seismic phenomenon that belongs to the slow earthquake family. Unlike regular earthquakes, it is characterized by a small amplitude, long duration, and no clear arrivals of P and S waves [Peng and Gomberg, 2010]. However, tremor, similar to regular earthquakes, is likely generated by shear slip and in many cases associated with GPS-based observations of slow-slip events (SSEs) [Obara, 2011; Wech and Creager, 2011]. Tremor and SSEs, which are stress sensitive, can be triggered by regional and teleseismic earthquakes [Nadeau and Guilhem, 2009; Peng and Gomberg, 2010; Zigone et al., 2012; Chao et al., 2013]. Since tremors and SSEs are located below the seismogenic zone, where large earthquakes nucleate, they may provide important information on stress variation before the occurrence of large nearby earthquakes [Obara and Kato, 2016].

Recent studies have found that nearby earthquakes can affect tremor and SSE activities. For example, after the occurrence of moment magnitude (M_w) 6.0+ earthquakes in Central California and southern Taiwan, nearby tremor activity exhibits a long-term increase in the tremor rate, likely resulting from an increase in static Coulomb stress caused by the main shocks [Nadeau and Guilhem, 2009; Shelly and Johnson, 2011; Chuang et al., 2014]. A recent study of the interaction between tremor and nearby intraslab earthquakes in the Nankai subduction zone in southwestern Japan suggests that tremor is more likely triggered by earthquakes than vice versa [Han et al., 2014]. In comparison, a recent observation in New Zealand indicates that one M_w 6.3 earthquake arrested a nearby ongoing SSE [Wallace et al., 2014].

While the above studies present evidence on how earthquakes affect tremor and SSE activity, other recent studies have focused on the influence of tremor and SSEs on local earthquake activity. For example, Vidale et al. [2011] showed that an episodic tremor and slip event in the Cascadia subduction zone triggered several small-magnitude earthquakes in nearby regions. Shelly [2009] reported that 3 months before the 2004 M_w 6.0 Parkfield earthquake, several tremor families exhibited unidirectional migration accompanied by an elevated

tremor rate. *Nadeau and Guilhem* [2009] found intense tremor activity ~3 weeks before the 2004 Parkfield event. Other studies have indicated that ongoing SSEs may have preceded the rupture of several M_w 8.0+ megathrust earthquakes [*Ito et al.*, 2013; *Kato and Nakagawa*, 2014]. *Colella et al.* [2017] observed increases in microseismicity a few weeks prior to the 2012 M_w 7.4 Ometepc earthquake in the Oaxaca region of southern Mexico. However, these SSEs were based on observations from GPS or micro-earthquakes such as repeating earthquakes or foreshock/swarm sequences. While it has been suggested that the frequent occurrence of tremor and SSEs may trigger large earthquakes if the locked region is critically stressed [e.g., *Obara and Kato*, 2016], we still lack strong evidence of aseismic deformation change before large earthquakes [*Roeloffs*, 2006].

Many studies based on observations [*Bouchon et al.*, 2013; *Kato and Nakagawa*, 2014], laboratory experiments [*Selvadurai and Glaser*, 2015], and modeling [*Avouac*, 2015] have suggested slow aseismic slip during the pre-nucleation process of a fast-rupturing earthquake. Such an aseismic process could increase stress in surrounding areas and trigger foreshocks [*Ohnaka*, 1992; *Bouchon et al.*, 2013; *Ito et al.*, 2013; *Kato and Nakagawa*, 2014]. However, observing such pre-nucleation processes in the field is relatively difficult [*Roeloffs*, 2006]. In addition, other studies have suggested that foreshocks [*Helmstetter and Sornette*, 2003] and aftershocks [*Felzer et al.*, 2002] have similar triggering mechanisms without an accompanying aseismic process.

An ideal region for examining the relationship between tremor and nearby earthquakes is Taiwan. Situated at the boundary between Eurasia and the Philippine Sea Plate, Taiwan is seismically active with frequent occurrences of moderate to large earthquakes. In addition, several recent studies have identified tremor triggered by teleseismic earthquakes [*Peng and Chao*, 2008; *Chao et al.*, 2012, 2013], ambient tremor that occurs naturally in the same region [*Chuang et al.*, 2014; *Idehara et al.*, 2014; *Sun et al.*, 2015] beneath the southern Central Range.

The focus of this paper is to quantify ambient tremor activity before and after the 4 March 2010 M_L 6.4 Jiashian earthquake that occurred in the southern Central Range of Taiwan [*Ching et al.*, 2011]. We selected this earthquake because the epicenter of the Jiashian main shock was located about 20 km southwest of active, triggered/ambient tremor sources (Figure 1a) [*Chao et al.*, 2013; *Chuang et al.*, 2014; *Sun et al.*, 2015]. In addition, the M_w 8.8 Maule, Chile earthquake, which occurred on 27 February 2010, triggered micro-earthquakes, ice quakes, tremor, and SSEs around the world [*Peng and Gombert*, 2010; *Peng et al.*, 2010, 2014; *Zigone et al.*, 2012]. Hence, this sequence provides an ideal data set for analyzing the relationship between tremor and large, local, teleseismic earthquakes.

2. Automatic Tremor Detection Procedure

The seismic data used in this study were recorded by short-period (1 Hz) seismometers in the Central Weather Bureau Seismic Network (CWBSN) [*Shin et al.*, 2013] and the Broadband Array in Taiwan for Seismology (BATS). All stations are equipped with three-component sensors, and the sampling rates are 100 Hz for CWBSN and 20 Hz for BATS. The analyzed time window was from 1 January 2009 to 31 December 2011.

Our analysis procedure mainly consisted of two steps. First, using the waveform envelope correlation and clustering (WECC) method [*Wech*, 2010], we obtained a preliminary event catalog that included coherent tremor signals and other nontremor sources. Then we applied a spatiotemporal clustering criterion [*Maeda and Obara*, 2009; *Obara*, 2010] to separate tremor episodes from regular earthquake signals and other unknown sources. To evaluate the robustness of detection, we obtained an initial tremor catalog of episodes of tremor durations longer than 10 min by visually examining 6 months of data from 1 January 2010 to 30 June 2010 and compared them with those of another tremor catalog [*Chuang et al.*, 2014]. After we optimized the auto-detection procedure to include these long-duration tremor episodes, the algorithm selected shorter isolated tremor events based on the criteria defined in section 2.2.

2.1. Automatic Tremor Detection With the WECC Algorithm

We began the process by selecting 10 seismic stations that recorded triggered [*Peng and Chao*, 2008; *Chao et al.*, 2012] and ambient tremor [*Chao et al.*, 2013] with high signal-to-noise ratios and a reasonable geographical distribution around the tremor source region (Figure 1a). Then we applied a 2–8 Hz band-pass filter on

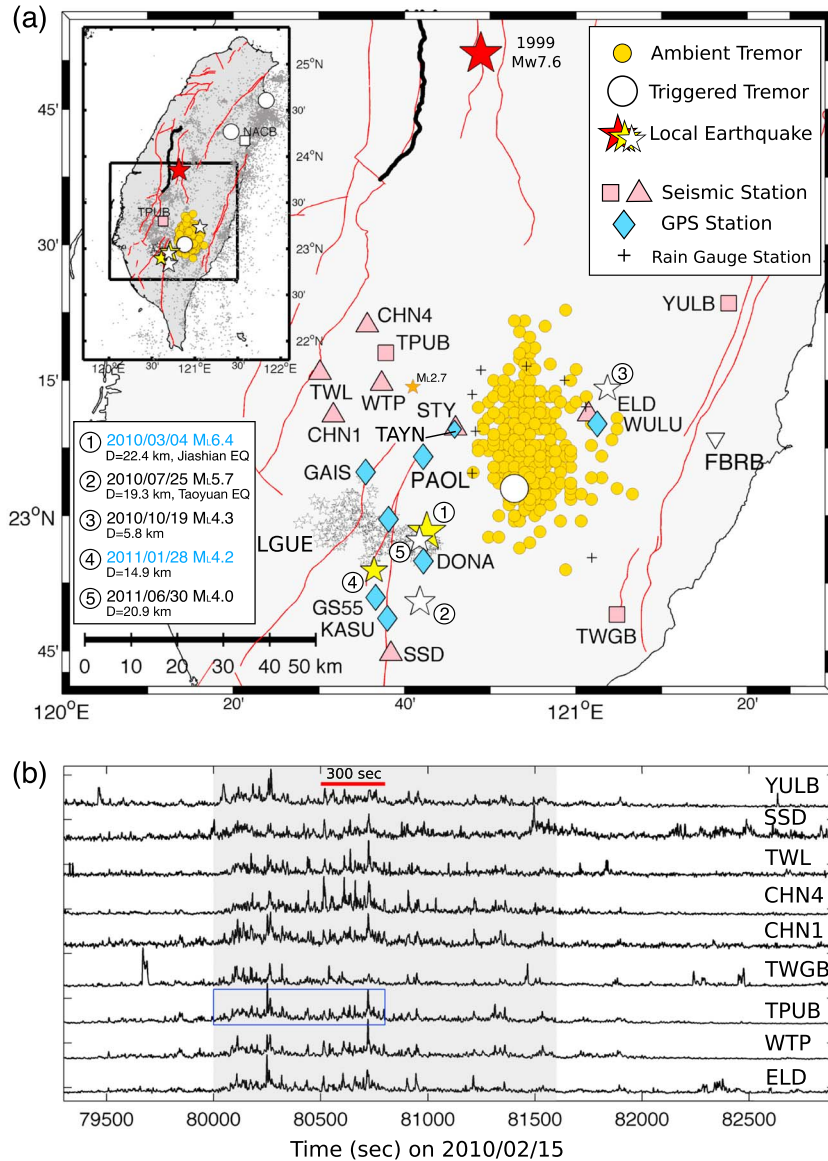


Figure 1. (a) Map of the study region in the southern Central Range of Taiwan. The small gold circles mark all detected tremor episodes during the 3 year study period (1 January 2009 to 31 December 2011) that spanned 14 months before and 22 months after the 4 March 2010 M_L 6.4 Jiashian earthquake (event #1, star symbol). Each circle of tremor represents one average location for a continuous tremor episode with a duration time between 6 and 43 min. The Jiashian main shock and its aftershock sequences (i.e., 4 March 2010 to 10 March 2010) are denoted by large yellow and small open stars, respectively. Other nearby earthquakes with M_L (local magnitude) greater than 4.0 are marked with identification numbers from #2 to #5 (Table S1). The thin and thick lines indicate local faults and the rupture zone of the 1999 M_w 7.6 Chi-Chi earthquake (red star), respectively. The large open circles mark triggered tremor sources of the 11 March 2011 M_w 9.0 Tohoku-Oki earthquake [Chao *et al.*, 2013]. Local seismicity from the relocated CWB (Central Weather Bureau) earthquake catalog [Shin *et al.*, 2013] (1 January 2010 to 30 June 2010) is denoted by small dots shown in the insert panel. The 10 stations used for locating tremor in this study are denoted by squares and triangles for the broadband BATS and short-period CWB stations. The 4 March 2010 M_L 2.7 earthquake occurring about 14 min before the Jiashian main shock is marked by an orange star (Figure 7o). Volumetric strainmeter station FBRB is denoted by a white inverted triangle (Figure S6). (b) One hour 2–8 Hz band pass-filtered envelope seismograms (starting at 22:01:40 on 15 February 2010, UTC) illustrating ambient tremor recorded in an E component recorded by surrounding stations. The gray shadow region marks the detection of tremor episodes with a duration of ~27 min. The 360 s scale bar represents the shortest duration time for each continuous tremor episode required in this study. The blue rectangle marks the same 800 s long ambient tremor seismogram shown in Figure 2a.

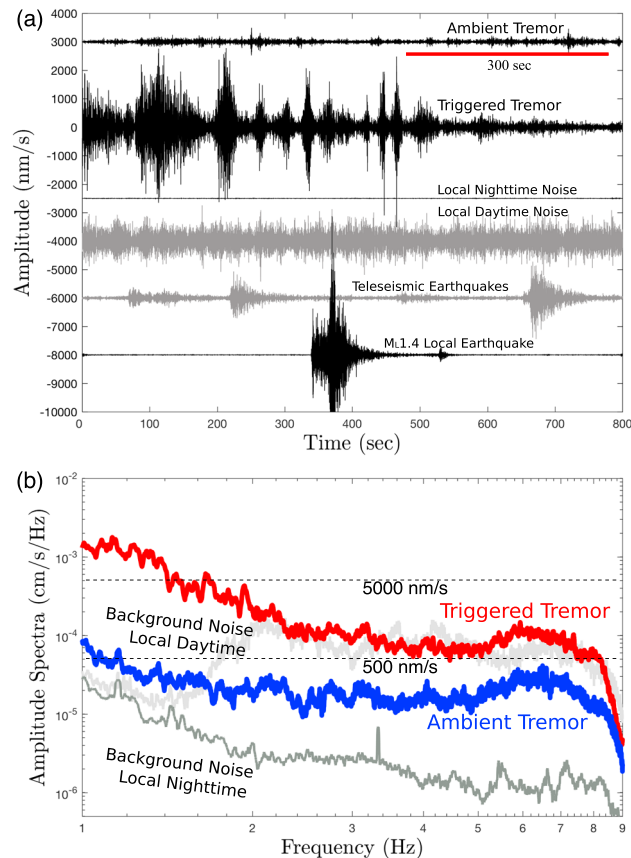


Figure 2. (a) Comparisons of amplitude for types of seismic sources at broadband station TPUB (from top to bottom): ambient tremor (i.e., the same TPUB records shown in Figure 1b by a blue rectangle), triggered tremor [Chao *et al.*, 2013], local nighttime noise, local daytime noise, teleseismic earthquakes from the aftershocks of the 2011 M_w 9.0 Tohoku-Oki earthquake, and a local M_L 1.41 earthquake. All seismograms are observed at broadband station TPUB in the E component on 2–8 Hz band pass-filtered instrument-corrected velocity seismograms. Detailed event information can be found in Table S2a. (b) A comparison of stacking spectra for ambient tremor (blue), triggered tremor (red), local nighttime background noise (dark gray), and local daytime background noise (light gray). Each type of spectrum was stacked with four to seven events from instrument-corrected velocity seismograms in the E component at broadband station TPUB. Detailed event information can be found in Table S2b. The two horizontal dotted lines mark the maximum amplitude threshold for the ambient tremor (500 nm/s) and the triggered tremor (5000 nm/s) used in this study.

the E component, generated the envelope function, applied a low-pass filter at 0.1 Hz, and down-sampled the envelope seismogram to 1 Hz at 10 stations for further analysis [Wech, 2010]. We chose the E component because tremor mainly contains S wave energy evident on the horizontal components and assumed that tremor was associated with shear slip because of nearly E-W compression [Chao *et al.*, 2012]. Figure 1b illustrates ambient tremor with nonimpulsive and long-duration coherent signals among many surrounding stations. Next, we used a 2 min time window to cross-correlate envelope seismograms with a 50% time overlap. The time window was shorter than the 5 min window used in Cascadia [Wech, 2010], mostly due to the more frequent occurrence of earthquakes in Taiwan than in Cascadia (i.e., on average 28 earthquakes of $M_L \geq 2$ daily and 3.5 earthquakes of $M_L \geq 6$ annually between 2004 and 2011) [Shin *et al.*, 2013]. With a shorter time window for autoscanning, we were more easily able to separate tremor from earthquakes (Figure 2a and supporting information Table S2) with the spatiotemporal clustering criterion (section 2.2).

We then used the WECC procedure to estimate the location of each 2 min time window from S wave lag times with envelope correlation coefficient (CC) values of ≥ 0.75 by performing a 3-D grid search with a 1-D velocity model around the tremor sources [Tang *et al.*, 2010]. We based our choice of $CC \geq 0.75$ on the test results of

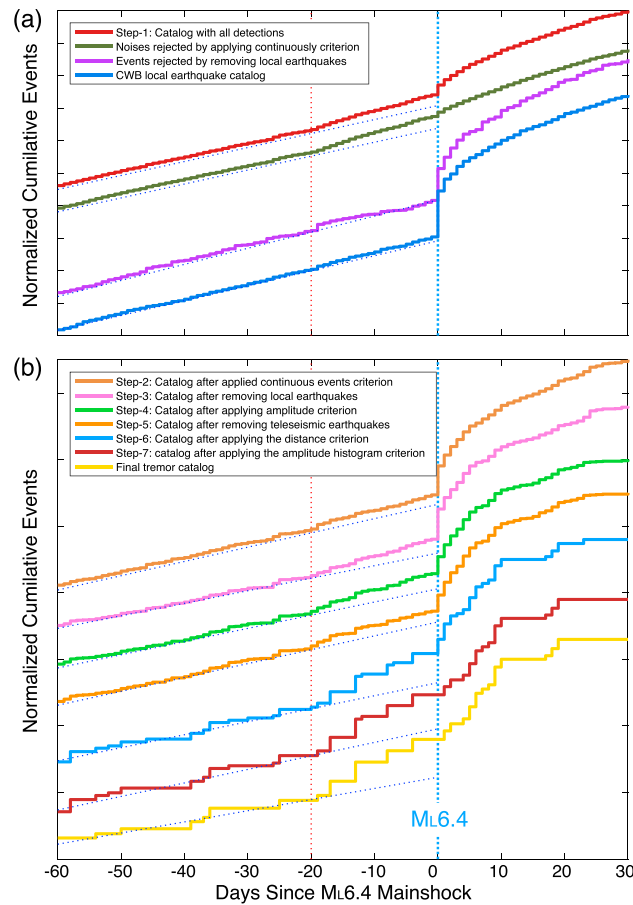


Figure 3. (a, b) Statistical results of cumulative events for various selection stages of catalogs and events for removing earthquakes and noise. The dotted line shows the best fitting line with data observed between -60 and -20 days. The blue vertical dotted line indicates the occurrence of the $M_L6.4$ main shock. The red vertical dotted line marks a reference time of -20 days.

2010]. This step contained the following three selection criteria (Figure 3): (1) using earthquake catalogs and reference station criteria for removing local and distant earthquakes, (2) adapting an amplitude threshold criterion, and (3) considering each tremor cluster as continuous events in time and space. We began by identifying local and regional earthquakes that occurred during potential tremor episodes, as listed in the Central Weather Bureau (CWB) catalog [Shin et al., 2013]. To remove the aftershock sequences of teleseismic earthquakes (Figure 2a), we applied a reference station criterion [Kim et al., 2011] to earthquakes of $M_w \geq 6.5$ with minimum theoretical dynamic stress of ≥ 1.5 kPa measured at broadband station TPUB. Specifically, we selected detected events that occurred after 31 selected teleseismic main shocks from the ANSS (Advanced National Seismic System) earthquake catalog (Table S3) and cross-correlated the envelope seismograms of station TPUB and a reference station, NACB, located in northern Taiwan, ~ 144 km away from the tremor sources (insert of Figure 1a). If the correlation coefficient value of the envelope similarity between these two stations was higher than 0.75, we assumed that the coherence signal originated from a teleseismic earthquake and rejected it. After this step, we removed 7691 detection windows for local earthquakes and 1558 for regional and teleseismic earthquakes.

After removing potential local and distant earthquakes, we applied an amplitude threshold criterion to remove possible small local earthquakes that appeared on seismograms but that were not listed in the CWB catalog. Using 2–8 Hz filtered envelope functions at stations TPUB and TWGB (Figure 1a), we measured the maximum amplitude during each 2 min time window. Because the amplitude of tremor is generally small

the tremor detection rate (Figure S1) from known tremor observations [Chao et al., 2013]. For each 2 min window that passed the CC criterion, we used bootstrap error estimation by randomly removing 10% of the data to obtain one location and repeating the same procedure in as many as 10 tentative locations with the same time window. Then we obtained one median horizontal location for each 2 min window with epicentral error estimation of less than 5 km. Although the WECC algorithm calculated the depth at each location, in this study, we did not search for tremor depth because of the considerable uncertainty [Wech, 2010; Wech and Creager, 2011]. During this step, the detection of WECC may include tremor, local or regional earthquakes, and other known high-frequency sources (Figure S2). From the 3 year data set, we identified 100,988 2 min detections.

2.2. Spatiotemporal Clustering Criterion

To remove high-amplitude earthquake signals and low-amplitude unknown sources, we applied a spatiotemporal clustering criterion [Maeda and Obara, 2009; Obara,

and varies only slightly with size [Vidale *et al.*, 2011], we set a threshold of 500 nm/s to separate tremor from earthquake signals. This empirical amplitude threshold is based on visual examinations of tremor waveforms during the 6 month (January 2010 to June 2010) period, resulting in an average of 251 ± 136 nm/s, similar to the amplitudes from another study [Yabe *et al.*, 2014]. After applying the amplitude criterion, we rejected another 2640 events.

As mentioned before, large distant earthquakes, which have been well studied in Taiwan, can trigger tremor [Peng and Chao, 2008; Chao *et al.*, 2012]. As triggered tremor has a much larger amplitude than ambient tremor (Figure 2), we applied a higher amplitude threshold of 5000 nm/s, double the maximum triggered tremor amplitude observed between 2004 and 2008 [Chao *et al.*, 2012], during the occurrence of tremor-triggering events. During the analyzed time period of 2009–2011, only the 11 March 2011 $M_w 9.0$ Tohoku-Oki earthquake satisfied this criterion, so we retained the associated tremor (Figure S3b) [Chao *et al.*, 2013].

We define a tremor episode as a cluster of tremors lasting at least 5 min, which translates to at least four detections of 2 min tremor events with 1 min overlap (Figures 1b and S2h), also spatially clustered. In addition, to avoid contamination of earthquake signals or simultaneous activations of multiple tremor sources, we limited the epicentral distance between 2 min events to 60 km (Figure S3). Our underlying assumption is that a local small earthquake or any unknown source is typically an isolated event (or followed by sporadic aftershocks). The generation of a signal lasting over 5 min is highly unlikely (Figures S2 and S3). By applying this criterion, we rejected 86,128 detection windows with isolated events of smaller amplitude earthquakes, noise, and other unknown sources (Figure 3). To further confirm each detection, we also calculated the amplitude histogram of the detection window. Since an earthquake typically generates an impulsive signal, the maximum value of the 1 sigma standard deviation of an amplitude histogram for an earthquake typically yields a higher value than that of tremor within a given time window (Figure S3). Hence, we set a threshold of 12 times the standard deviation above the mean and rejected another 546 events with maximum values above this threshold (Figure S3c).

After the automatic detection and selection procedures, we obtained 2425 two minute events and 338 clustered episodes (Figure 4), which is $\sim 2.4\%$ of the original 2 min detections. We also visually examined the waveforms of each tremor episode (e.g., Figure S3) and found that 97.9% of the clustered events (i.e., 331 out of 338 episodes) were real detections of tremor. Figure S4 illustrates the remaining seven events that we did not include in the final clustered tremor catalog. They include typical earthquake signals with impulsive arrivals of *P* and *S* waves (i.e., Figures S4a–S4e) and other unknown isolated events (Figures S4f–S4g) that were not removed by our selection procedures.

3. Observations of Tremor Activity

3.1. Tremor Catalogs

For the purpose of interpreting tremor activity as described below, we obtained two types of tremor catalogs that we categorized into the following:

1. *The 2 min catalog* (Table S4). This catalog provides detailed information such as the location and the amplitude of each detected 2 min event. The catalog contains 2425 two minute events (Figure 4c), some of which include isolated detections not listed in the clustered catalog.
2. *The clustered catalog* (Table S5). This catalog includes 331 clustered episodes observed in 205 days during the 3 year study period (Figures 1a and 4a). Although one daily tremor episode represents mostly continuously occurring tremor activity from 6 to 42 min, some episodes might have been interrupted by earthquake signals (e.g., Figure S2h). The average location and amplitude of each tremor episode were calculated from the mean of all 2 min events. This catalog, used in subsequent sections, reveals temporal changes in the tremor rate before and after the Jiashian earthquake.

3.2. General Features of Ambient Tremor

Our newly detected ambient tremor occurs beneath the southern Central Range. It is located in the same region as the triggered tremor (i.e., white circle in Figure 1a) [Peng and Chao, 2008; Chao *et al.*, 2012, 2013] but covers a wider area, particularly in the north-south directions. The spectrum of ambient tremor shares

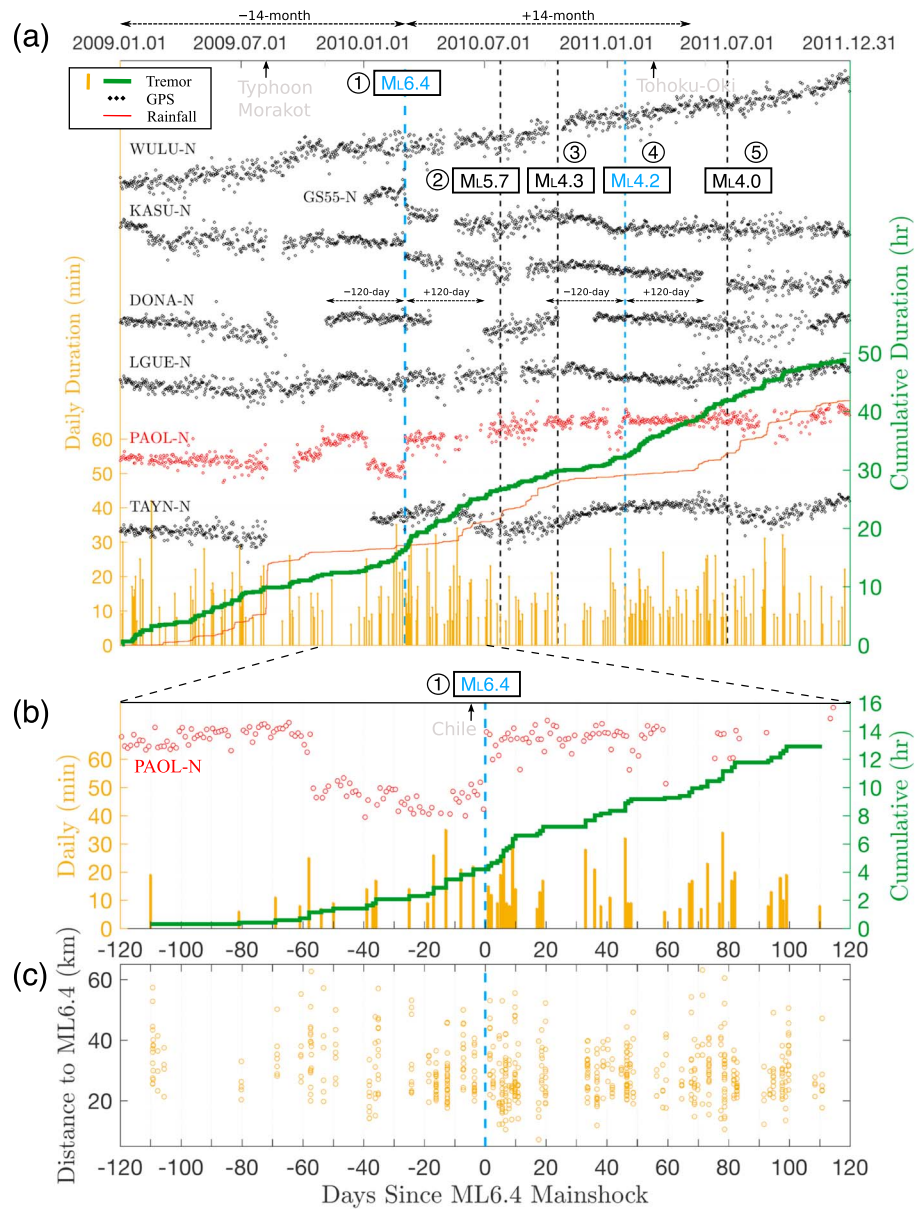


Figure 4. (a) Ambient tremor activity in the southern Central Range during a 3 year period (1 January 2009 to 31 December 2011) before and after the local 4 March 2010 $M_L6.4$ Jiashian earthquake (event #1, vertical blue dotted line). The gold-enrod-colored bars (left y axis) denote the daily concurrence time of tremor. The green solid line (right y axis) indicates the cumulative duration of tremor. The black and red circles show the daily GPS records. The vertical arrows mark the typhoon Morakot and the tremor-triggering event of the 11 March 2011 $M_w9.0$ Tohoku-Oki earthquake. (b) 120 day tremor activity before and after the Jiashian earthquake. The vertical arrow marks the 27 February 2010 $M_w8.8$ Chile earthquake (no triggered tremor). Other notations are the same as those in Figure 4a. (c) The epicentral distance to the Jiashian main shock epicenter for all individual 2 min tremor events.

a pattern similar to that of triggered tremor, but it has lower amplitudes (Figure 2b). The total daily duration of tremor was between 6 and 42 min, and the daily mean and median durations were 14.4 and 13 min, respectively. About 95.7% of tremor episodes occurred during the local nighttime (i.e., 19:00 to 06:00, Figure 5a), suggesting that our tremor catalog likely misses many events during the local daytimes.

To quantify the recurrence period of tremor, we computed the time interval between consecutive days with tremor listed in the clustered catalog. Most of the recurrence times were equal to or less than 5 days (141 episodes, or 68.8% of all episodes), and only eight episodes (or 3.9% of all episodes) has longer recurrence times

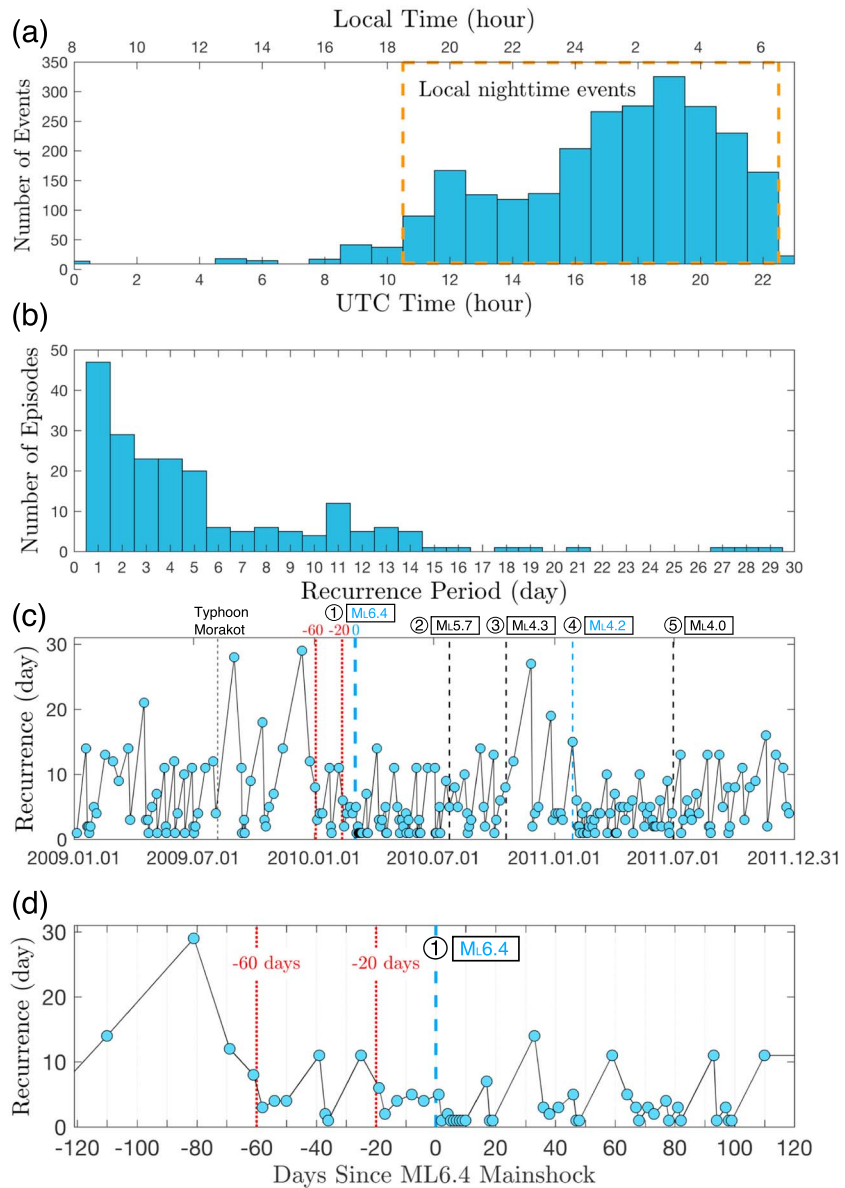


Figure 5. (a) The 24 h tremor distribution plot for all tremor episodes observed in this study. The 12 h local nighttime corresponds to 19:00–07:00 local time (i.e., UTC time between 11:00 and 23:00). Up to 96% of tremor episodes were observed during the local nighttime. (b) The histograms of the tremor recurrence time by computing the interval between consecutive days with tremor activity. (c) The temporal variation of the tremor recurrence time for the entire study period. (d) The tremor recurrence time of 120 days before and after the Jiashian main shock.

ranging from 15 to 29 days (Figure 5b). The average daily tremor recurrence period was 5.3 days, and the median value was 4 days (Figure 5b). Overall, while tremor occurred more frequently on some days than on others, we found no discernible recurrence pattern from our 3 year data set (Figures 5c and 5d).

3.3. Tremor Activities After and Before the Jiashian Earthquake

Similar to *Chuang et al.* [2014], we found a long-term increase in the tremor rate after the 4 March 2010 M_L 6.4 Jiashian earthquake based on the cumulative duration time for the clustered catalog (green line in Figure 4a). In the 14 month period following the main shock, the total duration time of tremor increased 35.3% over the same length of time before the main shock (i.e., from 16.3 to 22.1 h). Several studies observed a similar pattern in Central California after the 2004 M_w 6.0 Parkfield earthquake

[Nadeau and Guilhem, 2009; Shelly and Johnson, 2011], suggesting that static shear stress changes from main shock slip and afterslip were the most responsible for triggering tremor in this region. Therefore, to compute the change in Coulomb stress after the Jiashian main shock, we employed two faulting models (i.e., the low-angle thrust fault model and the high-angle reverse fault model) as a receiver fault based on the tremor focal mechanism observed by Ide *et al.* [2015]. Coulomb stress calculations from both fault models showed an increase in static Coulomb stress in the tremor zone at depths between 25 km and 35 km (Figure 6), which are generally consistent with the majority of tremor depths observed by Ide *et al.* [2015] (a depth range of 20–45 km) and Aguiar *et al.* [2017] (a depth range of 18–33 km).

Tremor also appears to have increased about 19 days before the Jiashian main shock (hereafter, –19 days) (Figures 4a and 4b). The average daily tremor durations are 12.6 ± 5.5 min. (i.e., observations from –6 months to –20 days) and 14.4 ± 6.9 min. (i.e., observations from –60 days to –20 days). Compared to 22.6 ± 9.4 min. (average from –19 days to 0 days), the corresponding increases are 44.2% or 36.3%, respectively. To further confirm that the increase in the tremor rate did not depend on our clustering selection criteria, we compared the output tremor events from –60 to +30 days during each step of the tremor selection criteria (Figure 3). As expected, the distribution of removed events exhibits temporal patterns similar to that of the earthquake activity listed in the CWB earthquake catalog (purple and blue lines in Figure 3a). The cumulative number of aftershocks within 10 days after the $M_L 6.4$ Jiashian main shock shows a typical decaying pattern that differs from the linearly increasing pattern of the cumulative tremor events (a line of the final tremor catalog in Figure 3b). Also, during each stage after the removal of the various types of nontremor signals, the cumulative events show a pattern of an increasing rate between –20 and 0 days. Thus, we suggest that our observations of a long-term increase in the tremor rate after the Jiashian main shock and a short-term increase beforehand are robust. In other words, our selection criteria aided in the extraction of tremor signals from active earthquake signals and background noise. Additionally, we have examined all seismograms for detected tremor and confirmed that the detections indeed correspond to tremor episodes instead of other nontremor-type events (Figure 7).

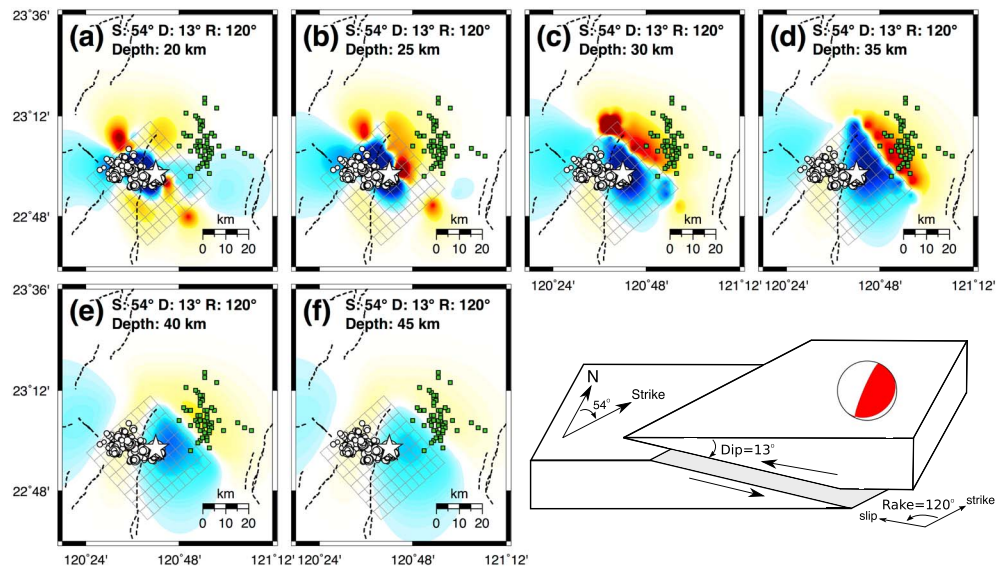
To quantify the statistical significance of changes in the tremor rate, we computed the β values [Matthews and Reasenber, 1988; Wu *et al.*, 2011] with various lengths of sliding windows (i.e., 5, 10, 15, and 20 days) of the entire data set from the clustered catalog (colored bars in Figure 4a). The β value is defined by $\beta = [N_a - (N_b + N_a) \cdot T_a / (T_b + T_a)] / \sqrt{(N_b + N_a) \cdot [T_a / (T_b + T_a)] \cdot [1 - T_a / (T_b + T_a)]}$, where T_b and T_a are time windows before and after the reference times, respectively, and N_b and N_a are the number of tremor events observed in each time window. We use the same length of time window (i.e., $T_b = T_a = 5, 10, 15, \text{ or } 20$ days) before and after each reference time, so the β value can be simplified as $\beta = [2N_a - (N_b + N_a)] / \sqrt{(N_b + N_a)}$. The β value results indicate short-term increases (i.e., for β values greater than 2) in the tremor rate before the main shock with sliding time windows of 10 days (Figure S5d), 15 days (Figure S5f), and 20 days (Figure S5h) even though an increase in the tremor rate also appeared during other time periods.

To examine possible correlations with changes in the tremor rate, we also included other data sets (i.e., rainfall data, background earthquake activity, and strainmeter data). From meteorological stations surrounding the tremor sources (i.e., the plus symbols in Figure 1a), we found no heavy rainfall in the last 60 days before the main shock, except for a slight increase that occurred on –20 days (i.e., the red line in Figure 4a). The largest rainfall signal was associated with the 2009 Typhoon Morakot (Figures 4a, S9, and S11). We also found no significant earthquake activity changes within 60 days before the Jiashian main shock, except for a subtle increase in the earthquake rate between –20 and 0 days (blue line in Figure 3a). A strainmeter at station FBRB, located in the Longitudinal Valley [Hsu *et al.*, 2015] to the east of the tremor zone (Figure 1a), did not show significant variation associated with an increase in the tremor rate (Figure S6).

3.4. Tremor Activity Associated With Teleseismic Earthquakes

Our automatic tremor detection algorithm also detected triggered tremor during the passing surface waves of the 11 March 2011 $M_w 9.0$ Tohoku-Oki earthquake (Figure S3b). The 2011 Tohoku-Oki main shock generated ~ 0.85 cm/s peak ground velocities at the TPUB station on the transverse component,

(a-f): The Low-Angle Thrust Fault Model



(g-l): The High-Angle Reverse Fault Model

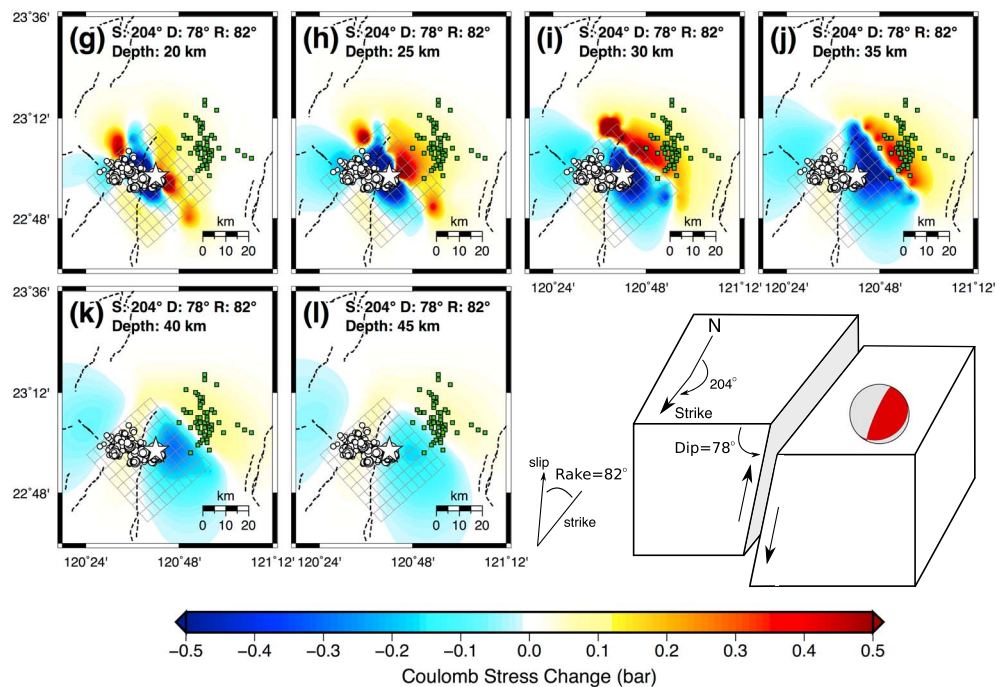


Figure 6. Coulomb stress changes following the 4 March 2010 M_L 6.4 Jiashian earthquake around the tremor sources. We used two faulting models as the receiver fault at tremor sources with a strike in the north northeast and south southwest directions and fault dipping to the east southeast [Ide et al., 2015]: (a–f): the low-angle thrust fault model (strike: 54°, dip: 13°, and rake: 120°) and (g–l): the high-angle reverse fault model (strike: 204°, dip: 78°, and rake: 82°) at depths of 20, 25, 30, 35, 40, and 45 km. The 40 × 50 km grid indicates the fault size of the Jiashian earthquake (strike: 318.05°, dip: 41.39°, rake: 40.29°, the top depth of the fault: 0.4102 km, and the bottom depth of the fault: 33.4693 km) [Ching et al., 2011]. The green squares mark tremor episodes that occurred within 120 days following the main shock.

corresponding to ~62 kPa dynamic stress [Chao et al., 2013]. Although the amplitude of triggered tremor is approximately 10 times as strong as that of ambient tremor, the spectra of triggered and ambient tremor exhibit similar shapes between 2 and 8 Hz (Figure 2). However, for frequencies less than 2–3 Hz, the spectral amplitude of ambient tremor becomes smaller than that of triggered tremor, and the shapes of the spectra

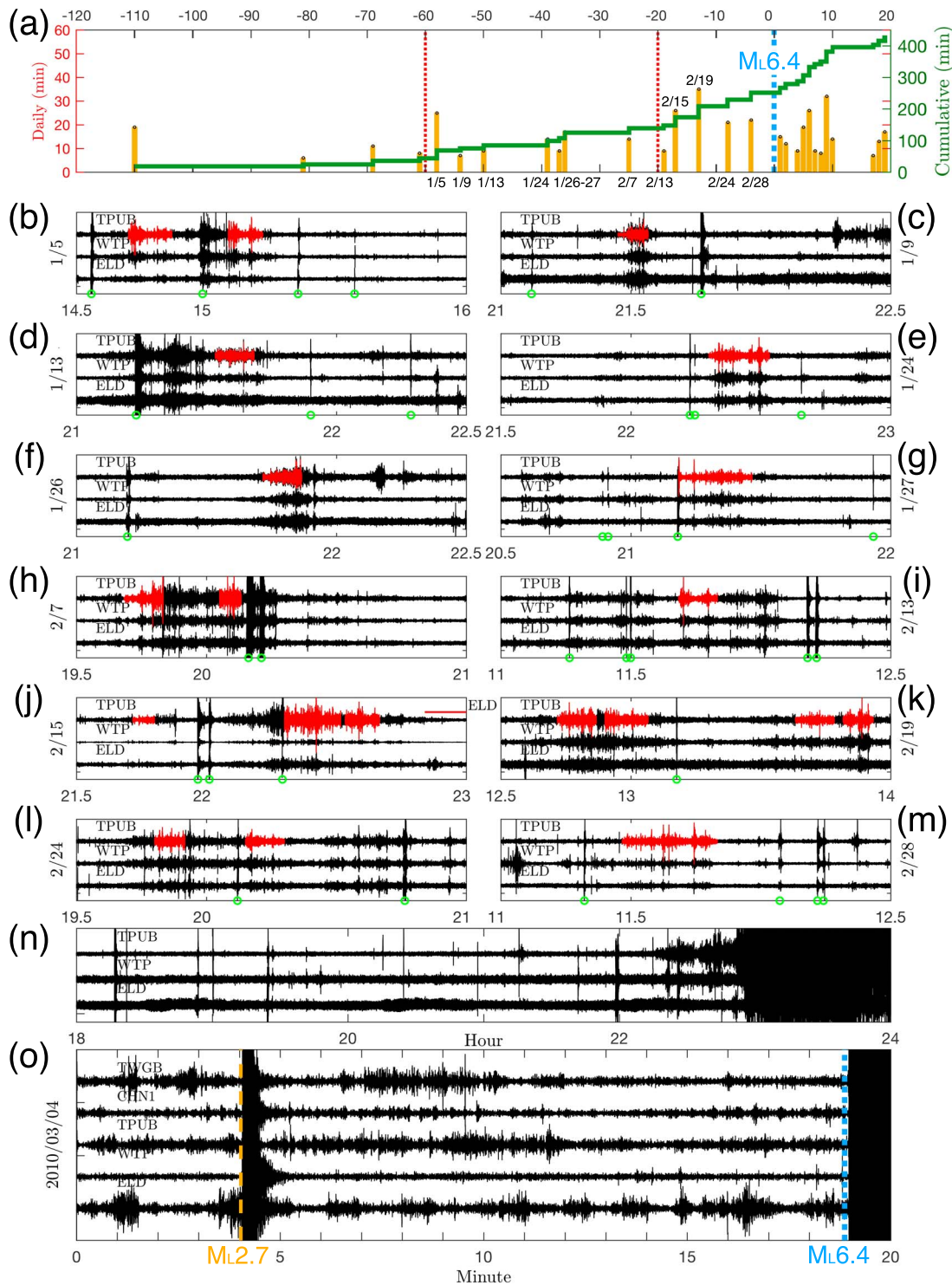


Figure 7. (a) Sixty day tremor activity before the 4 March 2010, 00:18:52.11, $M_L 6.4$ Jiashian earthquake. (b–m) The observed tremor (in red) within 60 days of the main shock. (n) An example of 6 h seismograms on 3 March 2010, showing no tremor observations before the main shock. (o) Twenty minute seismogram showing no tremor activity before the Jiashian earthquake. A local $M_L 2.7$ earthquake (~30 km north of the main shock epicenter) occurring 15 min before the main shock is marked in Figure 1a.

differ [Rubinstein *et al.*, 2010]. This finding confirms previous assumptions that triggered tremor originates from the same patches of ambient tremor, except that the occurrence probability of triggered tremor becomes elevated due to stress caused by surface waves [Chao *et al.*, 2013; Chao and Obara, 2016].

Compared to the M_w 9.0 Tohoku-Oki earthquake, the 27 February 2010, M_w 8.8 Chile earthquake (5 days before the Jiashian main shock, Figure 4b) generated a maximum dynamic stress of ~ 12 kPa (on the transverse component), which was higher than the inferred tremor-triggering threshold (i.e., 7–8 kPa) in this region [Chao *et al.*, 2012]. However, even though this event occurred within a period in which the tremor rate increased, we did not find any triggered tremor during passing surface waves with either the autodetecting system or our visual examination method (Figure S7) [Chao *et al.*, 2012, 2013].

4. GPS Analysis

4.1. Procedure for GPS Data Analysis

To quantify whether tremor activity is associated with observable episodic SSEs under the southern Central Range, we examined global positioning system (GPS) data during the 3 year study period. We used the GAMIT10.42/GLOBK5.16 software package [Herring *et al.*, 2010] to process the GPS data and double-differenced ionosphere-free carrier phase observations (L3) as primary observables. To obtain a more accurate and consistent regional deformation pattern in Taiwan, we used continuous three-component GPS data from 362 sites in Taiwan, 8 sites in Ryukyu, and 17 international global navigation satellite systems services (IGS) sites in the Asia-Pacific region [Hsu *et al.*, 2011] to align our regional solutions with the 2005 International Terrestrial Reference Frame (ITRF2005) coordinates [Altamimi *et al.*, 2007].

To obtain a final GPS position time series, we first removed station coordinates with enormous standard deviations (i.e., greater than 10 times the standard deviation within a given time window). Next, we performed a least squares regression to station position time series with regard to station velocity, annual and semiannual periodic motions, postseismic relaxation, and offsets caused by coseismic jumps and instrument changes. Then we carefully examined residuals and removed outliers that were more than two iterations from the least squares fit. Finally, we selected GPS stations within 100 km of central active tremor sources (Figure 1) and compared GPS daily position time series to daily tremor activity (Figures 4 and S9).

4.2. GPS Observations

From the 3 year data set, we identified no consistent correlation between the GPS trend and tremor rates (Figure 4a), but we did identify a temporal relationship between changes in the GPS and the rate of tremor before the Jiashian earthquake (Figure 4b). Starting at about -60 days, the N-S component at the PAOL station began to exhibit a dramatic decline (i.e., toward the south). This significant change, however, appeared only at the N-S component of the PAOL station, but the E-W component of PAOL and other station components exhibited very subtle changes (Figure S9). This component continuously moved southward at around -40 and -20 days and then shifted northward between -20 and 0 days, which was close to the time when the rate of ambient tremor began to increase (Figure 4b). Although the variation between -20 and 0 days was also recorded by other surrounding GPS stations such as in GS55, the changes were much smaller than those observed at PAOL. During other time periods, however, the correlations between changes in the GPS trend and increases in the tremor rate were inconsistent.

4.3. GPS Modeling

To reveal the potential underlying faulting mechanism and the location responsible for the increase in tremor activity, we modeled GPS data between -60 and 60 days in time intervals of every 20 days (Figure 8). To obtain constrained modeling results, we included stations that had recorded clear temporal variation (i.e., TAYN, PAOL, LGUE, DONA, and GS55) and other stations over in a wider area (i.e., GAIS, S012, GS52, MLO1, KASU, LIKN, and WULU). We estimated GPS horizontal displacements over 20 day time periods using a least squares function. Since the deformation signal was subtle, and it did not allow us to constrain all of the fault parameters, we fixed the fault length and width to be 10 km and used a NW-SE striking fault plane dipping 40° to the NE so that it was consistent with the main shock rupture. We obtained the best fitting model by a grid search for the location of the fault.

Our modeling results do not show any constrained and stable fault slip beneath the southern Central Range during this time period (Figure 8). In addition, depending on the selection of stations by the bootstrap method, the source location may vary since changes in our target signals over a 20 day period were too subtle to be captured by all surrounding GPS stations (Figures 1, 4, and S9). Nevertheless, while the best fitting sources of faulting were mostly located west of the tremor zone for -60 to $+60$ days (Figure 8), the

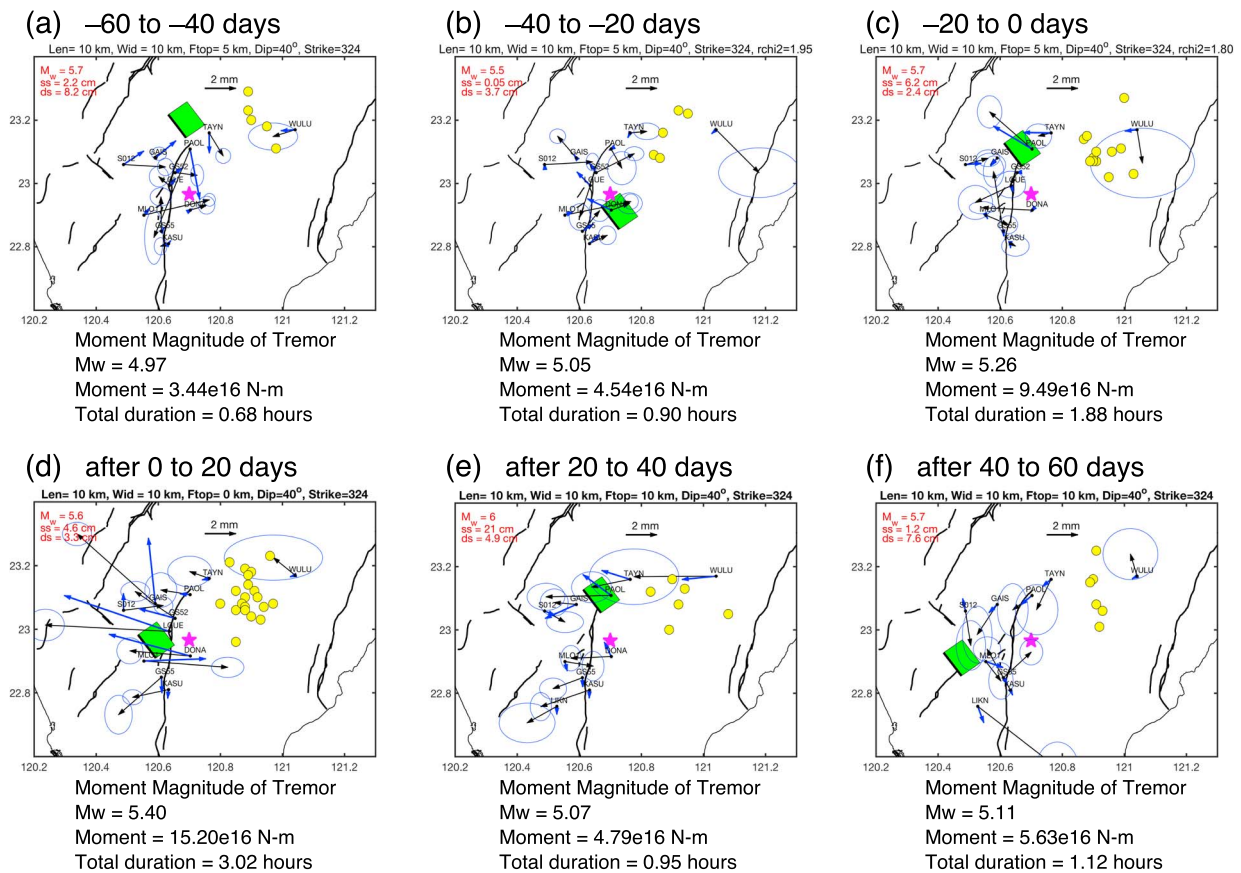


Figure 8. Modeling results for the GPS data. The green square represents the best fitting faulting source with GPS observations. The abbreviations: Len (fault length), Wid (fault width), Ftop (depth of the fault top), rchi2 (reduced chi-square), ss (strike-slip component, left-lateral slip is considered positive), and ds (dip-slip component, thrust slip is considered positive). The yellow circles indicate tremor locations from the clustered catalog. The moment magnitude of tremor in each 20 day period is computed by the total duration of tremor activity [Aguiar *et al.*, 2009].

source of tremor from -40 to -20 days was close to the epicenter of the Jiashian main shock with a 10 km depth. The equivalent moment magnitudes of the faulting sources ranged from M_w 5.5 to M_w 6.0.

5. Discussion

5.1. Potential Bias of the Tremor Detection Algorithm

In this study, we developed a robust algorithm for the automatic detection and location of tectonic tremor beneath the southern Central Range of Taiwan. Unlike other regions (e.g., Japan and Parkfield) with sensitive borehole stations, our study relied only on the use of surface stations. Because of the strong amplitude of background noise recorded during the local daytime (Figures 2 and 5), some ambient tremor could have gone undetected [Maeda and Obara, 2009]. In addition, our spatiotemporal clustering criterion may have excluded potential isolated events or weak tremor episodes. However, confirming whether these isolated or short-duration events were signals from tremor or other unknown sources was difficult. Hence, it is important to note that this catalog did not include most daytime tremor activity and other weak tremor episodes. Nonetheless, it can still provide useful information on the spatiotemporal evolution of tremor activity in the southern Central Range.

As mentioned before, due to large uncertainties in the WECC method [Wech, 2010], our tremor catalog did not include depth information. In subduction zones, many studies have simply projected tremor epicenters onto plate interfaces [Obara, 2010; Wech and Creager, 2011]. However, because of the lack of definitive information on source faults for generating tremor in our study region, we were unable to perform such projection. Ide *et al.* [2015] suggested that the focal mechanism of low-frequency earthquakes (LFEs) beneath the

southern Central Range is consistent with a low-angle thrust fault. Another recent study of LFE locations indicated a near-vertical, distributed pattern in the tremor source region [Aguar *et al.*, 2017] consistent with that found by previous studies of triggered LFEs [Tang *et al.*, 2010] and ambient tremor in this region [Chuang *et al.*, 2014]. Hence, the fault geometry responsible for hosting tremor beneath the southern Central Range remains unclear.

5.2. Lack of Triggered Tremor During the 2010 Chile Main Shock

To explore why no tremor was triggered by the 2010 Chile event, we compared the surface waves and spectra of the triggering (2011 Tohoku-Oki) and nontriggering (2010 Chile) events (Figure S8). We found that the large amplitudes of Love and Rayleigh waves of the 2011 Tohoku-Oki event lasted longer (i.e., more than 700 s, Figure S8b) than those of the 2010 Chile event (i.e., ~300 s, Figure S8a). In addition, the largest dynamic stress measured from the Chile event, 12 kPa, appeared at only one cycle of the Rayleigh wave, and the remaining surface waves did not generate dynamic stress that exceeded the tremor-triggering threshold. Thus, we suggest that even though dynamic stress plays a significant role in dynamic triggering, the frequency content and duration of the surface waves or body waves also play a significant role in controlling the tremor-triggering threshold [Aiken *et al.*, 2013]. Moreover, since the Chile main shock did not trigger any instantaneous tremor during its surface waves or tremor rate changes at slightly longer times (i.e., no tremor was observed within ± 12 h), we inferred no causal link between the Jiashian main shock and the Chile earthquake.

5.3. No Clear Long-Term GPS-Observable SSEs Associated With Tremor Activity

By comparing tremor in the southern Central Range of Taiwan to other tectonic environments, Idehara *et al.* [2014] suggested that Taiwan tremor patches occurred in a small rupture area with short durations. Our observations also indicated that tremor activity beneath the southern Central Range had a short duration (an average of 14.4 min per day) and short-recurrent cycle (an average of 5.3 days) and that it did not correlate with GPS-observable SSEs. If we assume that the occurrence of any ambient tremor represents an ongoing SSE [Wech and Creager, 2011], the estimated magnitude of SSEs beneath the southern Central Range would be small because of the short duration of tremor activity [Idehara *et al.*, 2014]. Such small-magnitude SSEs (i.e., magnitude less than $M_w 5.5$, Figure 8) would probably not generate slip large enough to be recorded by GPS stations [Obara, 2011]. For example, even in the tectonic tremor-active region along the Parkfield-Cholame sections of the San Andreas Fault in California, no direct GPS or strainmeter observable SSEs associated with tremor activities have been detected [Smith and Gomberg, 2009]. Similarly, we suggest that the southern Central Range is unlikely to produce larger-magnitude SSEs associated with tremor (Figure 8).

5.4. Tremor Activity Before the Jiashian Earthquake

To reveal a plausible correlation between sudden changes in GPS displacement observed at -60 days associated with tremor activity (Figure 4b), we first checked the field GPS station at PAOL to confirm that the changes were real signals rather than false detections. We found that during the study period, no antenna had been replaced, except following typhoon Morakot (~7 months before the Jiashian main shock, Figure 4a). If we assume an association between a GPS-observable event and a sudden slip at depth, surface deformations recorded at many surrounding stations should have ensued. However, while a clear drop at -60 days appeared at the N component of the PAOL station, only a coherent but smaller variation was observed in the E component of the PAOL and other stations (Figures 4a and S9). Moreover, we cannot obtain a constrained faulting model that fits GPS records that show a significant change at the N component of PAOL along with subtle changes in other stations (Figure S9). Thus, we suggest that the sudden change at -60 days could have resulted from a very localized signal, not an ongoing deep SSE around the study region. The PAOL site, located on a river terrace, experienced insignificant motion, even during heavy rain or typhoons (Figure 4a). Hence, we also exclude the possibility that this change was caused by shallow landslides or other transient signals.

Below we evaluate both positive and negative evidence that the increasing tremor rates in the last few weeks before the Jiashian main shock reflected aseismic slip. First, changes in the tremor rate closely matched changes in the N-S component of the GPS PAOL station (Figures 4 and S9). As mentioned before, tremor is extremely stress sensitive, and it can be perturbed by small stress variations on the order of several kilopascals from various external stress perturbations. Thus, we can reasonable assume that precursory aseismic slip

in the lower crust may have caused stress changes, starting at -19 days, in the eventual rupture zone of the Jiashian main shock. In addition, the long-term trends exhibited in GPS records before and after the Jiashian main shock are consistent with those of (i.e., cumulated regional stress moving toward the northwest) *Ching et al.* [2011]. *Ching et al.* [2011] also suggested that triggered tremor from *Peng and Chao* [2008] was likely located in the downward extension of the epicenter of the Jiashian main shock. However, changes in the tremor rates and GPS vectors before the Jiashian main shock could be coincidental. We note that only the GPS PAOL station showed clear signals at -60 days and immediately before the main shock (Figures 4 and S9). Despite some coherent signals at nearby stations (e.g., LGUE and DONA), they were much weaker than those at the PAOL station. Hence, the best fitting models in these time periods (-60 to -40 , and -20 to 0 days) were likely just beneath PAOL (Figures 8a and 8c) rather than near either the Jiashian main shock nucleation zone or the tremor region. The best fitting slip patch between -40 and -20 days was near the main shock nucleation zone. However, tremor was not very active during this time period. Finally, we also checked but did not find any clear migration pattern of tremor activity right before the main shock (Figure S10). Hence, while the tremor rates changed before the Jiashian main shock, we were unable to geodetically observe aseismic slip preceding the main shock. This finding indicates that aseismic slip did not occur or that it did occur but remained undetected by surface GPS stations.

5.5. Tremor Activity Associated With Other Nearby Earthquakes

To further check whether temporal variations in the tremor rate and GPS records could be also observed during other earthquakes, we selected additional earthquakes with local magnitudes (M_L) greater than 4.0 surrounding the tremor source regions (Table S1). We compared the cumulative tremor rate, GPS records, and tremor recurrence cycles within 120 days before and after five selected earthquakes. As shown in Figure 9d, the 2011 $M_L4.2$ earthquake (Event #4, 14.9 km in depth), located in the Jiashian aftershock zone (Figure 1), exhibited a pattern similar to that of the Jiashian main shock (Figure 9a, Event #1, 22.4 km in depth) in several aspects: an increase in the long-term tremor rate after each main shock, a slight increase in tremor duration starting at -20 days, a change in the slip direction of GPS records between -30 and 0 days, and an increase in tremor recurrence cycles between -120 and -20 days (Figure 5c, periods before Events #1 and #4). In comparison, the 2010 $M_L5.7$ Taoyuan earthquake (Event #2, 19.3 km in depth), which occurred 143 days after the Jiashian earthquake (Figure 4) [*Chan and Wu*, 2012] exhibited no increase in tremor activity after the main shock. Since the occurrence times between these five earthquakes are relatively short (~ 121 days on average, Figure 4a), their impacts on changes between the tremor rates and the directions of surface slip of each earthquake are not easily distinguishable. For example, tremor became more active after Event #1, and the observations during $+20$ to $+120$ days in Figure 9a overlaps -120 to -20 days in Figure 9b. In other words, the Taoyuan earthquake occurred within the period while the tremor rate was still increasing due to the Jiashian main shock. Thus, the association between changes in the tremor rate and the Taoyuan earthquake is unclear. Another 2010 $M_L4.3$ shallow earthquake (Event #3, 5.8 km in depth) located to the north of the active tremor source and the 2011 $M_L4.0$ earthquake (Event #5, 20.9 km in depth) located next to the Jiashian hypocenter (Figures 9 and 1) also showed no significant changes in either the tremor rate or GPS records.

As for the increase in the tremor rates between -20 and 120 days for the Jiashian and $M_L4.2$ events (Figures 9a and 9d, respectively), we cannot rule out the possibility that they are not correlated with nearby earthquakes. One possibility could be rate decreases (or increases in recurrence cycles) of tremor activity between -120 and -20 days (Figures 9a and 9d, respectively), a few months after the 2009 Typhoon Morakot. However, we found that the recurrence times (the inverse of rates) in the last 20 days before the Jiashian main shock were even lower than the recurrence times before the Typhoon Morakot (Figures 5c and S11). An alternative explanation is that the decrease in tremor recurrence cycles (or higher tremor rates) may indicate a tremor source region closer to failure, and tremor activity would have been more sensitive to stress variation from a nearby earthquake.

6. Conclusion

In this study, we developed an automatic tremor detection and location algorithm and applied it to the southern Central Range of Taiwan. During the 3 year study period between 2009 and 2011, we obtained a

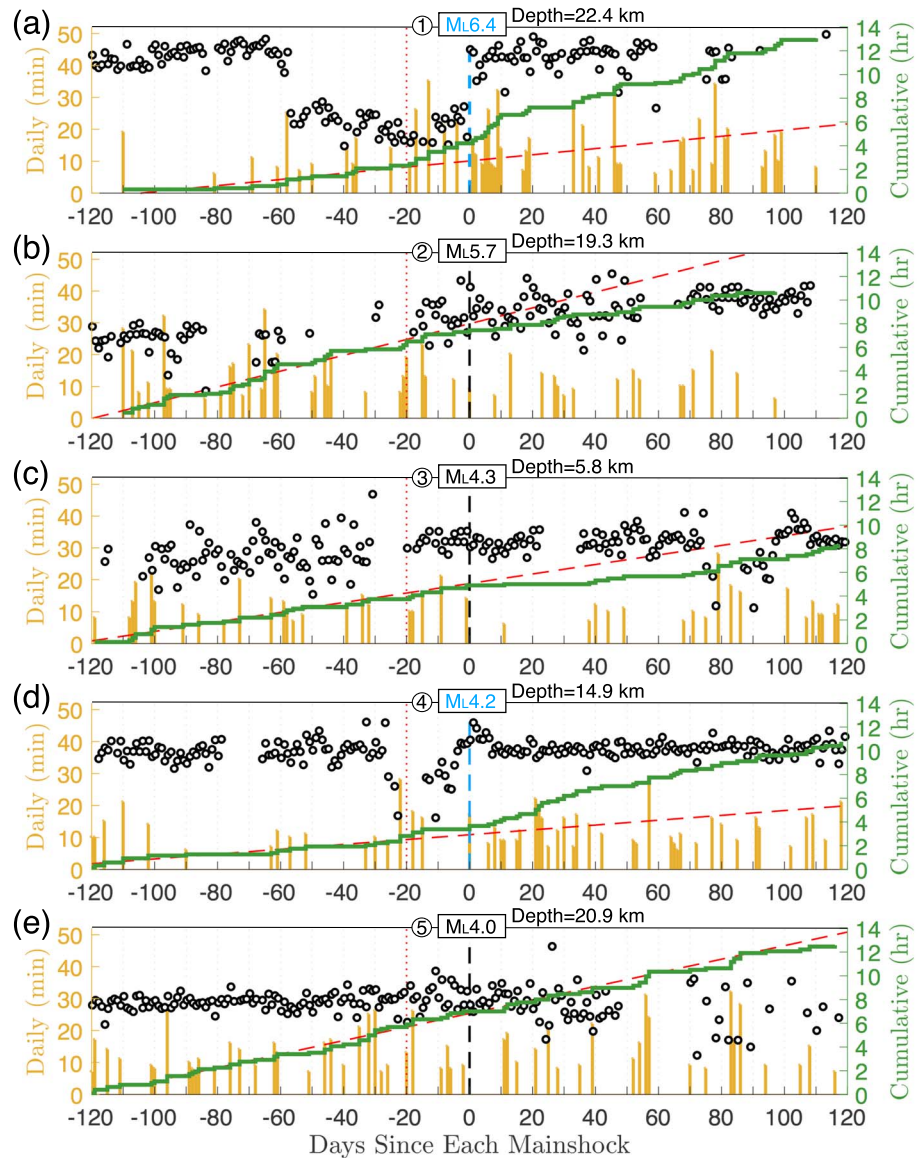


Figure 9. Comparison between the tremor rate and GPS records for 120 days before and after five selected earthquakes (Figure 1a and Table S1). Open circles mark GPS data observed at the PAOL station in the north component. The red dotted line indicates the best fitting line computed between -120 and -20 days. Figure 9a is the same as in Figure 4b for the Jiashian main shock.

robust tremor catalog with both ambient and triggered tremor. We found that ambient tremor activity in the southern Central Range had short durations (with a daily average of 14.4 min) and short recurrence periods (an average of 5.3 days). We also examined GPS data from stations surrounding the tremor sources and found no GPS-observable slow-slip events correlated with tremor activity. Our results also indicate that triggered tremor has a spectrum identical to that of ambient tremor, but with much larger amplitude, supporting previous findings that triggered tremor is the accelerated version of ambient tremor [e.g., Chao and Obara, 2016].

We also examined temporal variation of ambient tremor activity before and after the nearby 2010 $M_L 6.4$ Jiashian earthquake (i.e., 20 km away from tremor sources). We found that the tremor rate started to increase a few weeks before the Jiashian main shock and continued with a long-term increase after the main shock. The daily tremor duration time, starting at 19 days before the main shock, increased from 12.6 ± 5.5 min to 22.6 ± 9.4 min. Also, a nearby GPS station recorded a change in the N-S component at the same time as

the tremor rate began to increase. We also observed a similar temporal variation pattern in the tremor rate and GPS data before and after the 2011 M_L 4.2 earthquake. Since tremor is extremely stress sensitive, we suspect that the increase in the tremor rate may have reflected the aseismic pre-nucleation process of the nearby Jiashian earthquake. However, as only one station recorded geodetic signals, we were not able to determine reliable information about aseismic slip around the main shock epicenter. Hence, we assume that such an aseismic process did not occur or that it was too small to be recorded by surface GPS stations.

Compared with the same period before the main shock, the long-term tremor rate after the Jiashian earthquake increased by $\sim 35\%$. The following increase in the tremor rate was mainly due to the increase in static Coulomb stress in the surrounding regions after the Jiashian earthquake. In addition, although the 2010 M_w 8.8 Chile earthquake occurred 5 days before the Jiashian earthquake, we found no clear triggered tremor during its surface waves, suggesting no correlation among the 2010 Chile earthquake and tremor activity and the Jiashian earthquake.

Although our analysis provided a consistent tremor catalog from 2009 to 2011, it was limited to only surface seismic stations, resulting in high background noise during the local daytime, when the amplitude of noise is greater than that of ambient tremor. We suggest that future studies of tremor in this region should place stations closer to the tremor sources. Alternative solutions include high-density seismic arrays [e.g., Sun *et al.*, 2015] or borehole stations, both of which would enable more accurate recording of tremor signals with high signal-to-noise ratios, specifically the signals of events occurring during the local daytime.

Acknowledgments

We thank the Editor, Yehuda Ben-Zion, the Associate Editor, Satoshi Ide, the reviewer, Chung-Han Chan, and the second anonymous reviewer for their useful comments. We thank the Taiwan Central Weather Bureau (CWB) and the Institute of Earth Sciences (IES) at Academia Sinica in Taiwan for providing short-period CWBSN data (<http://gdms.cwb.gov.tw/>, permission required), broadband BATS data (<http://bats.earth.sinica.edu.tw/>), and the earthquake catalog (<http://gdms.cwb.gov.tw/>, permission required). Rainfall and strainmeter sites are operated by CWB and IES, respectively. We also thank Lindsay Yu-Ling Chuang, Chi-Chia Tang, and Kate Huihsuan Chen for preparing part of the seismic data and Yih-Min Wu for providing the relocated earthquake catalog of the Jiashian aftershocks. The manuscript benefited from comments by Teh-Ru Alex Song and Alan T. Linde. Chao and Peng were supported by the National Science Foundation through award EAR-0956051. Chao is currently supported by the Northwestern Institute for Complex Systems (NICO) and the Center for Optimization and Statistical Learning (OSL) at Northwestern University through the Northwestern Data Science Scholars Fellowship. Any use of trade, firm, or product names is for descriptive purposes only and does not imply endorsement by the U.S. Government.

References

- Aguiar, A. C., T. I. Melbourne, and C. W. Scrivner (2009), Moment release rate of Cascadia tremor constrained by GPS, *J. Geophys. Res.*, *114*, B00A05, doi:10.1029/2008JB005909.
- Aguiar, A. C., K. Chao, and G. C. Beroza (2017), Tectonic tremor and LFEs on a reverse fault in Taiwan, *Geophys. Res. Lett.*, doi:10.1002/2016GL072148.
- Aiken, C., Z. Peng, and K. Chao (2013), Tremors along the Queen Charlotte Margin triggered by large teleseismic earthquakes, *Geophys. Res. Lett.*, *40*, 829–834, doi:10.1002/grl.50220.
- Altamimi, Z., X. Collilieux, J. Legrand, B. Garayt, and C. Boucher (2007), ITRF2005: A new release of the International Terrestrial Reference Frame based on time series of station positions and Earth orientation parameters, *J. Geophys. Res.*, *112*, B09401, doi:10.1029/2007JB004949.
- Avouac, J.-P. (2015), From geodetic imaging of seismic and aseismic fault slip to dynamic modeling of the seismic cycle, *Annu. Rev. Earth Planet. Sci.*, *43*, 233–271.
- Bouchon, M., V. Durand, D. Marsan, H. Karabulut, and J. Schmittbuhl (2013), The long precursory phase of most large interplate earthquakes, *Nat. Geosci.*, *6*(4), 299–302, doi:10.1038/ngeo1770.
- Chan, C. H., and Y. M. Wu (2012), A seismicity burst following the 2010 M 6.4 Jiashian earthquake—Implications for short-term seismic hazards in southern Taiwan, *J. Asian Earth Sci.*, *59*, 231–239, doi:10.1016/j.jseae.2012.08.011.
- Chao, K., and K. Obara (2016), Triggered tectonic tremor in various types of fault Systems of Japan following the 2012 M_w 8.6 Sumatra earthquake, *J. Geophys. Res. Solid Earth*, *121*, 170–187, doi:10.1002/2015JB012566.
- Chao, K., Z. Peng, C. Wu, C.-C. Tang, and C.-H. Lin (2012), Remote triggering of non-volcanic tremor around Taiwan, *Geophys. J. Int.*, *188*(1), 301–324, doi:10.1111/j.1365-246X.2011.05261.x.
- Chao, K., Z. Peng, H. Gonzalez-Huizar, C. Aiken, B. Enescu, H. Kao, A. A. Velasco, K. Obara, and T. Matsuzawa (2013), A global search for triggered tremor following the 2011 M_w 9.0 Tohoku earthquake, *Bull. Seismol. Soc. Am.*, *103*(2b), 1551–1571, doi:10.1785/0120120171.
- Ching, K.-E., K. M. Johnson, R.-J. Rau, R. Y. Chuang, L.-C. Kuo, and P.-L. Leu (2011), Inferred fault geometry and slip distribution of the 2010 Jiashian, Taiwan, earthquake is consistent with a thick-skinned deformation model, *Earth Planet. Sci. Lett.*, *301*, 78–86.
- Chuang, L. Y., K. H. Chen, A. Wech, and W. Peng (2014), Ambient tremors in a collisional orogenic belt, *Geophys. Res. Lett.*, *41*, 1485–1491, doi:10.1002/2014GL059476.
- Colella, H., S. Sit, M. Brudzinski, and S. Graham (2017), Seismicity rate increases associated with slow slip episodes prior to the 2012 M_w 7.4 Ometepec earthquake, *Earth Planet. Sci. Lett.*, *464*, 35–45, doi:10.1016/j.epsl.2016.12.032.
- Felzer, K. R., T. W. Becker, R. E. Abercrombie, G. Ekström, and J. R. Rice (2002), Triggering of the 1999 M_w 7.1 Hector Mine earthquake by aftershocks of the 1992 M_w 7.3 Landers earthquake, *J. Geophys. Res.*, *107*(B9), 2190, doi:10.1029/2001JB000911.
- Han, J., J. E. Vidale, H. Houston, K. Chao, and K. Obara (2014), Triggering of tremor and inferred slow slip by small earthquakes at the Nankai subduction zone in southwest Japan, *Geophys. Res. Lett.*, *41*, 8053–8060, doi:10.1002/2014GL061898.
- Helmstetter, A., and D. Sornette (2003), Foreshocks explained by cascades of triggered seismicity, *J. Geophys. Res.*, *108*(B10), 2457, doi:10.1029/2003JB002409.
- Herring, T. A., R. W. King, and S. C. McClusky (2010), Documentation of the GAMIT GPS analysis software release 10.4, Massachusetts Inst. Technol.
- Hsu, Y.-J., S.-B. Yu, L.-C. Kuo, Y.-C. Tsai, and H.-Y. Chen (2011), Coseismic deformation of the 2010 Jiashian, Taiwan earthquake and implications for fault activities in southwestern Taiwan, *Tectonophysics*, *502*, 328–335, doi:10.1016/j.tecto.2011.02.005.
- Hsu, Y. J., Y. S. Chang, C. C. Liu, H. M. Lee, A. T. Linde, S. I. Sacks, G. Kitagawa, and Y. G. Chen (2015), Revisiting borehole strain, typhoons, and slow earthquakes using quantitative estimates of precipitation-induced strain changes, *J. Geophys. Res. Solid Earth*, *120*, 4556–4571, doi:10.1002/2014JB011807.
- Ide, S., S. Yabe, H.-J. Tai, and K. H. Chen (2015), Thrust type-focal mechanisms of tectonic tremors in Taiwan: Evidence of subduction, *Geophys. Res. Lett.*, *42*, 3248–3256, doi:10.1002/2015GL063794.

- Idehara, K., S. Yabe, and S. Ide (2014), Regional and global variations in the temporal clustering of tectonic tremor activity, *Earth Planets Space*, 66(1), 66, doi:10.5047/eps.2012.06.001.
- Ito, Y., et al. (2013), Episodic slow slip events in the Japan subduction zone before the 2011 Tohoku-Oki earthquake, *Tectonophysics*, 600, 14–26, doi:10.1016/j.tecto.2012.08.022.
- Kato, A., and S. Nakagawa (2014), Multiple slow-slip events during a foreshock sequence of the 2014 Iquique, Chile M_w 8.1 earthquake, *Geophys. Res. Lett.*, 41, 5420–5427, doi:10.1002/2014GL061138.
- Kim, M. J., S. Y. Schwartz, and S. Bannister (2011), Non-volcanic tremor associated with the March 2010 Gisborne slow slip event at the Hikurangi subduction margin, New Zealand, *Geophys. Res. Lett.*, 38, L14301, doi:10.1029/2011GL048400.
- Maeda, T., and K. Obara (2009), Spatiotemporal distribution of seismic energy radiation from low-frequency tremor in western Shikoku, Japan, *J. Geophys. Res.*, 114, B00A09, doi:10.1029/2008JB006043.
- Matthews, M. V., and P. A. Reasenberg (1988), Statistical methods for investigating quiescence and other temporal seismicity patterns, *Pure Appl. Geophys.*, 126(2–4), 357–372, doi:10.1007/BF00879003.
- Nadeau, R. M., and A. Guilhem (2009), Nonvolcanic tremor evolution and the San Simeon and Parkfield, California, earthquakes, *Science*, 325, 191–193, doi:10.1126/science.1174155.
- Obara, K. (2010), Phenomenology of deep slow earthquake family in southwest Japan: Spatiotemporal characteristics and segmentation, *J. Geophys. Res.*, 115, B00A25, doi:10.1029/2008JB006048.
- Obara, K. (2011), Characteristics and interactions between non-volcanic tremor and related slow earthquakes in the Nankai subduction zone, southwest Japan, *J. Geodyn.*, 52(3–4), 229–248, doi:10.1016/j.jog.2011.04.002.
- Obara, K., and A. Kato (2016), Connecting slow earthquakes to huge earthquakes, *Science*, 353(6296), 253–257.
- Ohnaka, M. (1992), Earthquake source nucleation: A physical model for short-term precursors, *Tectonophysics*, 211(1), 149–178, doi:10.1016/0040-1951(92)90057-D.
- Peng, Z., and K. Chao (2008), Non-volcanic tremor beneath the central range in Taiwan triggered by the 2001 M_w 7.8 Kunlun earthquake, *Geophys. J. Int.*, 175(2), 825–829, doi:10.1111/j.1365-246X.2008.03886.x.
- Peng, Z., and J. Gomberg (2010), An integrated perspective of the continuum between earthquakes and slow-slip phenomena, *Nat. Geosci.*, 3, 599–607, doi:10.1038/ngeo940.
- Peng, Z., D. P. Hill, D. R. Shelly, and C. Aiken (2010), Remotely triggered microearthquakes and tremor in central California following the 2010 M_w 8.8 Chile earthquake, *Geophys. Res. Lett.*, 37, L24312, doi:10.1029/2010GL045462.
- Peng, Z. G., J. I. Walter, R. C. Aster, A. Nyblade, D. A. Wiens, and S. Anandakrishnan (2014), Antarctic icequakes triggered by the 2010 Maule earthquake in Chile, *Nat. Geosci.*, 7(9), 677–681, doi:10.1038/ngeo2212.
- Roeloffs, E. A. (2006), Evidence for aseismic deformation rate changes prior to earthquakes, *Annu. Rev. Earth Planet. Sci.*, 34, 591–627, doi:10.1146/annurev.earth.34.031405.124947.
- Rubinstein, J. L., D. R. Shelly, and W. L. Ellsworth (2010), Non-volcanic tremor: A window into the roots of fault zones, in *New Frontiers in Integrated Solid Earth Sciences, International Year of Planet Earth*, edited by S. Cloetingh and J. Negendank, pp. 287–314, Springer, Berlin, doi:10.1007/978-90-481-2737-5_8.
- Selvadurai, P. A., and S. D. Glaser (2015), Laboratory-developed contact models controlling instability on frictional faults, *J. Geophys. Res. Solid Earth*, 120, 4208–4236, doi:10.1002/2014JB011690.
- Shelly, D. R. (2009), Possible deep fault slip preceding the 2004 Parkfield earthquake, inferred from detailed observations of tectonic tremor, *Geophys. Res. Lett.*, 36, L17318, doi:10.1029/2009GL039589.
- Shelly, D. R., and K. M. Johnson (2011), Tremor reveals stress shadowing, deep postseismic creep, and depth-dependent slip recurrence on the lower-crustal San Andreas fault near Parkfield, *Geophys. Res. Lett.*, 38, L13312, doi:10.1029/2011GL047863.
- Shin, T.-C., C.-H. Chang, H.-C. Pu, H.-W. Lin, and P.-L. Leu (2013), The geophysical database management system in Taiwan, *Terr. Atmos. Ocean. Sci.*, 24(1), 11–18, doi:10.3319/TAO.2012.09.20.01(T).
- Smith, E. F., and J. Gomberg (2009), A search in strainmeter data for slow slip associated with triggered and ambient tremor near Parkfield, California, *J. Geophys. Res.*, 114, B00A14, doi:10.1029/2008JB006040.
- Sun, W. F., Z. Peng, C. H. Lin, and K. Chao (2015), Detecting deep tectonic tremor in Taiwan with a dense Array, *Bull. Seismol. Soc. Am.*, 105(3), 1349–1358, doi:10.1785/0120140258.
- Tang, C.-C., Z. Peng, K. Chao, C.-H. Chen, and C.-H. Lin (2010), Detecting low-frequency earthquakes within non-volcanic tremor in southern Taiwan triggered by the 2005 M_w 8.6 Nias earthquake, *Geophys. Res. Lett.*, 37, L16307, doi:10.1029/2010GL043918.
- Vidale, J. E., A. J. Hotovec, A. Ghosh, K. C. Creager, and J. Gomberg (2011), Tiny intraplate earthquakes triggered by nearby episodic tremor and slip in Cascadia, *Geochem. Geophys. Geosyst.*, 12, Q06005, doi:10.1029/2011GC003559.
- Wallace, L. M., N. Bartlow, I. Hamling, and B. Fry (2014), Quake clamps down on slow slip, *Geophys. Res. Lett.*, 41, 8840–8846, doi:10.1002/2014GL062367.
- Wech, A. G. (2010), Interactive tremor monitoring, *Seismol. Res. Lett.*, 81(4), 664–669, doi:10.1785/gssrl.81.4.664.
- Wech, A. G., and K. C. Creager (2011), A continuum of stress, strength and slip in the Cascadia subduction zone, *Nat. Geosci.*, 4(9), 624–628, doi:10.1038/ngeo1215.
- Wu, C., Z. Peng, W. Wang, and Q.-F. Chen (2011), Dynamic triggering of shallow earthquakes near Beijing, China, *Geophys. J. Int.*, 185, 1321–1334, doi:10.1111/j.1365-246X.2011.05002.x.
- Yabe, S., A. S. Baltay, S. Ide, and G. C. Beroza (2014), Seismic-wave attenuation determined from tectonic tremor in multiple subduction zones, *Bull. Seismol. Soc. Am.*, 104(4), 2043–2059, doi:10.1785/0120140032.
- Zigone, D., et al. (2012), Triggering of tremors and slow slip event in Guerrero, Mexico, by the 2010 M_w 8.8 Maule, Chile, earthquake, *J. Geophys. Res.*, 117, B09304, doi:10.1029/2012JB009160.